




Research Article



## Design and Modeling of a High-Acceleration MEMS G-Switch

Farzad Yadegari <sup>1\*</sup> , Ali Mahdianikhotbesara <sup>2</sup>, M. Hossein Sehat <sup>3</sup><sup>1</sup>Department of Mechanical Engineering, Amirkabir University of Technology (Tehran Polytechnic), Tehran, P.O.B. a15875-4413, Tehran, Iran<sup>2</sup>School of Mechanical Engineering, College of Engineering, University of Tehran, P.O. Box 11155/4563, Tehran, Iran<sup>3</sup>Department of Mechanical and Aerospace Engineering, Missouri University of Science and Technology, Rolla, MO 65409

### Keywords

Acceleration,  
MEMS,  
G-switch,  
COMSOL,  
Finite element analysis.

### Abstract

Due to widespread advances in various industries and new technologies, micro-electro mechanical systems (MEMS) systems have increased in today's world. Applications of MEMS are typically in the production of electromechanical consequences with high production efficiency and volume and the lower production costs. In this paper, the design, modeling, and a detailed production process of a prototype of a high acceleration MEMS G-switch are discussed. The system configuration of this switch is equivalent to traditional sensors of the same class, consisting of a proof mass handled by four cantilever beams. The proposed model has the ability to respond to accelerations in the range of 0 to 100g (low-g levels) and tolerance to mechanical failure up to 30,000g (high-g levels) acceleration. In order to simulate and evaluate the performance of the designed sensor, COMSOL Multiphysics finite element analysis software has been used. The results show that the proposed model can be constructed due to its simple structure.

### 1. Introduction

In today's world, due to the widespread advances in various industries and new technologies, the use of micro-electro mechanical systems (MEMS) have increased. Applications of MEMS are generally in the production of electromechanical products with high production efficiency and volume with low production costs. [1]. These parts are made on a small scale and have many applications in various industries such as sensors [2–4], actuators [5–8], biomedical devices [9–11], etc. Novel methods such as additive manufacturing (AM) and micro-friction stir welding (FSW) can be used for fabrication of such components with high mechanical properties [12–32]. Acceleration measurement and the operation of a mechanism at a specified acceleration by microelectromechanical equipment is a widely used subject. An example of this is the accelerometers used in car

airbags. The typical acceleration measured in this category is about 2g. But in the aerospace and automotive industries, these sensors sometimes need to withstand accelerations in the 100g-100,000g range [32]. Therefore, the structures proposed for them are slightly different from those proposed for vehicle accelerometers. In this report, we get acquainted with the modeling process of one of these structures, which is capable of withstanding a shock of about 30000 g.

### 2. Mathematical Modeling

The purpose of this study is to design and model a high-acceleration G-switch. The structure design of this switch is similar to conventional sensors of the same level, consisting of a mass that is controlled by four cantilever beams. The schematic image of this design is shown in Figure 1.

\* Corresponding Author: Farzad Yadegari  
E-mail address: [farzadyadegari@aut.ac.ir](mailto:farzadyadegari@aut.ac.ir)

Received: 18 April 2022; Revised: 12 May 2022; Accepted: 18 May 2022  
<https://doi.org/10.52547/crpase.8.2.2783>

Academic Editor: **He Li**

Please cite this article as: F. Yadegari, A. Mahdianikhotbesara, M. H. Sehat, Design and Modeling of a High-Acceleration MEMS G-Switch, Computational Research Progress in Applied Science & Engineering, CRPASE: Transactions of Mechanical Engineering 8 (2022) 1–5, Article ID: 2783.

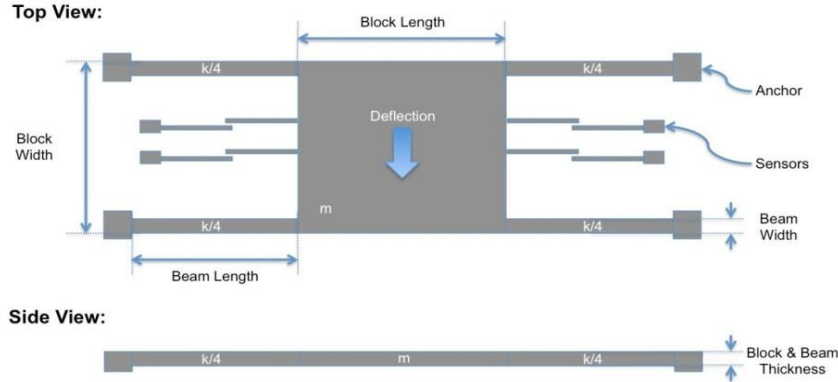


Figure 1. Schematic image of a sample G-switch design [32]

The following are the mathematical relationships associated with these design modeling [32]. If the force at acceleration  $a$  is  $F_a$ , this force is equal to the sum of the forces that are borne by the sensor beams ( $F_{s,sen}$ ) and the mass beams ( $F_{s,sup}$ ), i.e.:

$$F_a = F_{s,sen} + F_{s,sup} \quad (1)$$

By writing  $F_a$  in Eq. (1) in terms of the density ( $\rho$ ) of the material (silicon), the volume of the proof mass block ( $V_b$ ) and the maximum acceleration ( $a_m$ ) entered into it, as well as the force of the beams in terms of their stiffness, Eq. (2) can be written as:

$$\rho V_b a_m = k_{sup} x + k_{sen} (x - g) \quad (2)$$

where  $K$  is the stiffness equivalent to the beam,  $x$  is the amount of displacement from equilibrium, and  $g$  is the gap between the sensor beams before making contact. Also, return force of retaining beams is  $F_{res} = k_{sup} g$  and contact force at the point of impact of the sensor beams is  $F_{con} = F_{s,sen} = k_{sen} (x - g)$ .

According to Eq. (1) and Eq. (2), the force of the supporting beams can be rewritten as:

$$\begin{aligned} F_{s,sup} = k_{sup} x &= k_{sup} (x - g) + k_{sup} g \\ &= \frac{k_{sup}}{k_{sen}} F_{con} + F_{res} \end{aligned} \quad (3)$$

By substituting Eq. (3) in Eq. (2), the minimum possible value for the mass block volume is obtained:

$$V_b \geq \left( \frac{k_{sup}}{k_{sen}} + 1 \right) \frac{F_{con}}{\rho a_m} + \frac{(F_{res})_{min}}{\rho a_m} \quad (4)$$

Eq. (4) shows that the volume of the block depends on the stiffness of the whole beams (springs). Now, assuming that the maximum amount of deformation that occurs is equal to  $\delta$ , Eq. (5) can be written as:

$$\rho V_b a_s = k_{sup} (g + \delta) + k_{sen} \delta \quad (5)$$

where  $a_s$  acceleration due to maximum load is tolerable. Eq. (5) can be written as Eq. (6) to create a phrase similar to the left side of Eq. (2).

$$\rho V_b a_m = k_{sen} \left( \frac{k_{sup}}{k_{sen}} (g + \delta) + \delta \right) + \frac{a_m}{a_s} \quad (6)$$

Then by equating the right side, the Eq. (2) and Eq. (6) turn to:

$$\frac{k_{sup}}{k_{sen}} = \sqrt[3]{\frac{F_{res}}{F_{con}} \left[ \frac{a_s}{a_m} - \left( \frac{\delta}{g} + 1 \right) \right]^{-1} \frac{\delta}{g} + \frac{1}{4} \left\{ 1 + \frac{F_{res}}{F_{con}} + \left[ \frac{a_s}{a_m} - \left( \frac{\delta}{g} + 1 \right) \right]^{-1} \right\}^2} \sqrt{-\frac{1}{2} \left\{ 1 + \frac{F_{res}}{F_{con}} + \left[ \frac{a_s}{a_m} - \left( \frac{\delta}{g} + 1 \right) \right]^{-1} \right\}} \quad (7)$$

By considering the maximum strain equal to 0.008, which is common for such models, the size of the sensor and retaining beams can be calculated. Considering that the second deformation derivative ( $y''_{max}$ ) has a direct relationship with the flexural strain ( $\epsilon_{max}$ ) of the beams and that the mass retaining beams behave as a fixed-end beam due to their connection to the test mass, and the boundary conditions, the value of  $y''_{max}$  is created at both ends as in Eq. (8)

$$\epsilon_{max} = \frac{w_s}{2} y''_{max} = \frac{w_{sup} L_{sup} (F_{s,sup})_{max}}{4 E I_s n_{sup}} \quad (8)$$

where  $w_s$  is the width,  $L_{sup}$  is the length,  $I_s$  is the moment of inertia of the cross-section of the beams,  $n_{sup}$  is the number of supporting beams and  $E$  is the Young's modulus. On the other hand, the relationship between the stiffness of the supporting beams and their deformed state is shown in Eq. (9)

$$\frac{(F_{s,sup})_{max}}{n_{sup}} = \frac{k_{sup} x_{max}}{n_{sup}} = \frac{k_{sup} (g + \delta)}{n_{sup}} \quad (9)$$

and the expression of the stiffness of a fixed end beam is shown in Eq. (10)

$$\frac{k_{sup}}{n_{sup}} = \frac{12 E I_{sup}}{L_{sup}^3} \quad (10)$$

Now by substituting Eq. (10) in Eq. (9) and Eq. (8)

$$\epsilon_{max} = \frac{w_{sup}}{2} y''_{max} = \frac{3 w_{sup} (g + \delta)}{L_{sup}^3} \leq 0.008 \quad (11)$$

Eq. (11) is used to create the design range of the length and width of the retaining beams. By considering the amount of gap, the expression of stiffness can be written as Eq. (12)

$$\frac{k_{sup}}{n_{sup}} = \frac{(F_{s,sup})_{con}}{n_{sup}g} = \frac{\rho V_b a_m - F_{con}}{n_{sup}g} \quad (12)$$

Now the ratio of width to the length of the supporting beams is calculated as Eq. (13):

$$\frac{w_{sup}}{L_{sup}} = \sqrt[3]{\frac{\rho V_b a_m - F_{con}}{n_{sup}gEt_{sup}}} \quad (13)$$

where  $t_{sup}$  is the thickness of the beams, which according to the use of SOI wafer, this thickness is equal to the thickness of the block and in fact the thickness of the whole set. This relationship shows that in different cases, this ratio has a constant value. On the other hand, the solution to reduce the size of the sensor as much as possible is to reduce the length of the beams, which means that the minimum possible width for the beams should be selected and by determining the value of this parameter, the desired length of the beam is obtained.

The same is true for sensor beams as shown in Eq. (14) and Eq. (15):

$$\frac{k_{sen}}{n_{sen}} = \frac{12EI_{sen}}{L_{sen}^3} \quad (14)$$

$$\frac{w_{sen}}{L_{sen}} = \frac{k_{sen}}{n_{sen}t_{sen}E} \quad (15)$$

### 3. Finite Element Modeling

Recognizing the amount of acceleration and performing a specific operation (such as establishing an electrical circuit) at a specified acceleration is one of the tasks of a G-switch in the field of microelectromechanical systems. The purpose of this research work is to design and model a high acceleration G-switch. The structure design of this switch, similar to conventional sensors, consists of a proof mass that is controlled by four beams. Its schematic is shown in Figure 2.

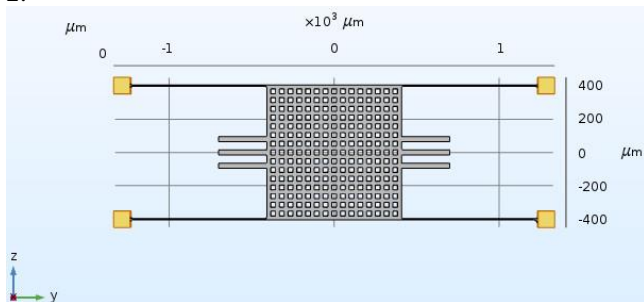


Figure 2. Geometric mechanism of the designed G-switch

As shown in Figure 2, the beams holding the proof mass are fixed at one end and attached to the proof mass at the other end, in which case they behave similarly to a fixed-end beam. This figure shows only the part related to the mechanics of the system that by applying acceleration in the z-direction, the proof mass is deformed and consequently, the sensor beams also experience the amount of displacement that the displacement intended by the design (here, this value is considered equal to 5 microns). Due to this displacement, a contact is established between the sensor

beams, and the target operation will be performed by establishing an electrical circuit.

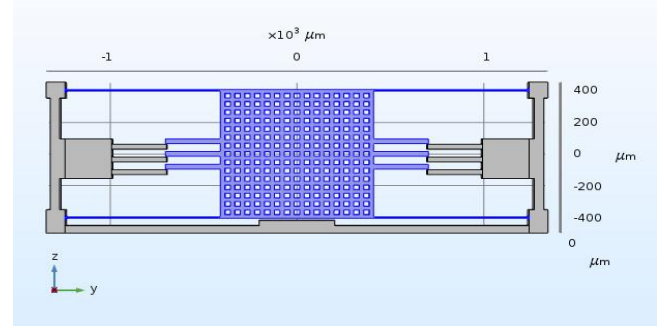


Figure 3. Geometry modeled for simulation in software

It should be noted that the geometry in Figure 3 has been created with the aim of having the ability to simulate in software. Because during the simulation process, importing components that are separate from each other seemed a bit difficult. But the main structure of the sensor that will be produced has only the components shown in Figure 4.

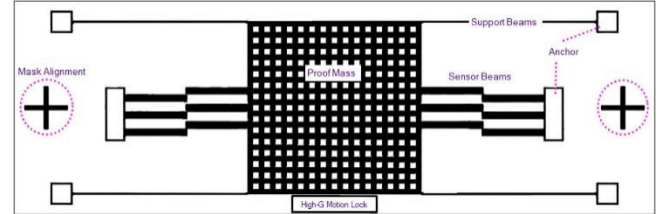


Figure 4. The main components of the G-switch are designed

After geometric modeling, accelerations of 70g and 3000g were applied in two stages to observe the sensor behavior. At 70g acceleration, an electric circuit is established by moving the mass to the gap intended for the sensor beams, and this sensor is capable of withstanding high accelerations up to about 30000g according to the simulation results. These results are shown in the two sections of stress and displacement in Figures 5 to 8. It should be noted that this stress will occur if the locking mechanism is not included in the simulation. Although the maximum amount of silicon stress is in the same range, in the case where the amount of movement is limited by the built-in lock, the resulting stress will be much less. This amount of displacement seems very high, despite the motion lock mechanism, such displacement will never occur, just as the simulation stress is not created by this lock.

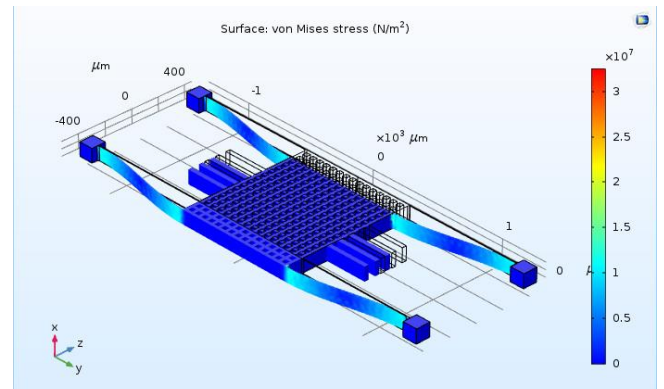
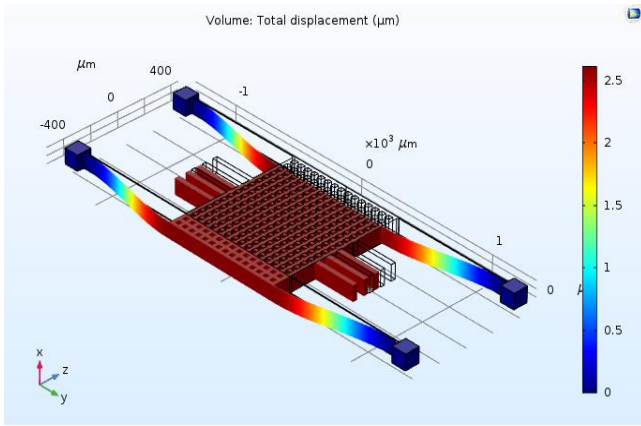
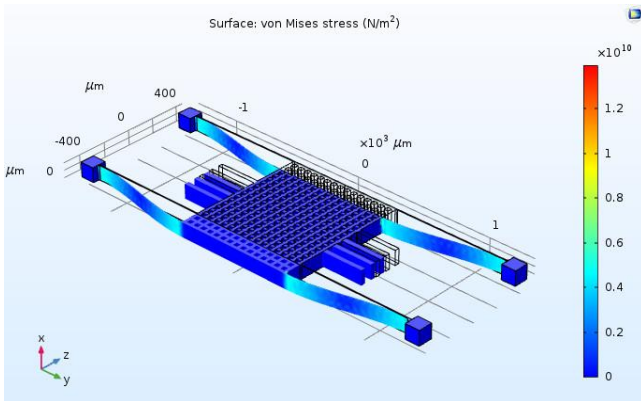


Figure 5. Stress distribution at 70g acceleration - Maximum stress value: 10 MPa



**Figure 6.** Displacement at 70g acceleration - Maximum amount of displacement: 2.6 microns



**Figure 7.** Stress distribution at of 30000g acceleration - Maximum amount of stress generated: 4000 MPa

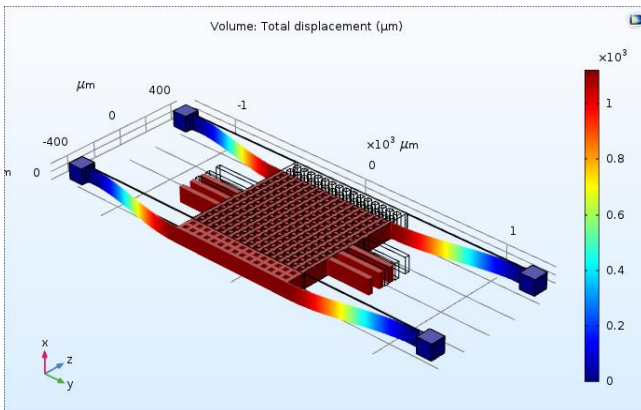


**Figure 8.** Degree of displacement at 70g acceleration - Maximum amount of displacement: 1.2 mm

#### 4. Electrical Circuit Design

In this section, an electrical circuit is designed to use the G-switch function. By applying the desired acceleration to the design and displacement of the sensor beams to the extent of the gap between them, the circuit is established and stimulates the desired operator. This operator, which depending on the need can be any mechanism, is specified in the circuit as a Device.

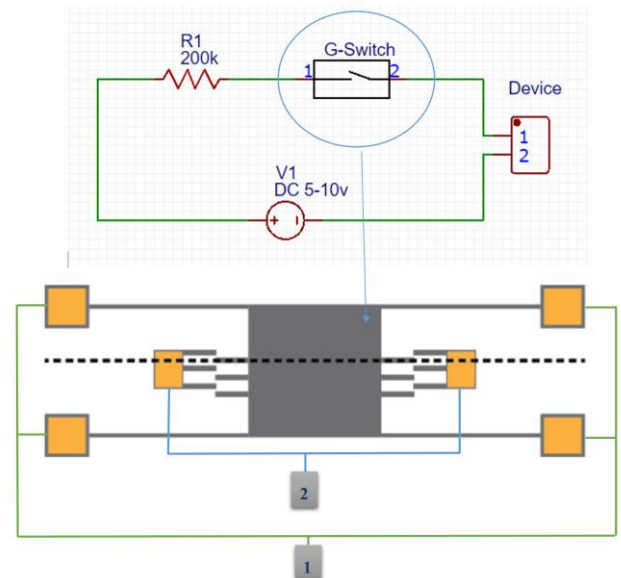


**Figure 9.** Circuit designed to operate the sensor and show how the components are connected

Due to the connection between the components, by making contact between the sensor beams, the circuit is established and then the Device will achieve its function. It is worth noting that this G-switch can be used with the help of gap changes between the sensor beams for accelerations up to 150g. But what was simulated in the initial design of this report was an acceleration of 70g.

#### 5. Conclusion

In this study, we designed a high-acceleration G-switch that is capable of delivering low-acceleration responses in the range of 0 to 100g and withstanding high-acceleration shocks of up to 30,000g without failure. Finite element simulation has been used to validate the design. The production process of this device is based on the use of SOI wafers. It is suggested that in future research, the causes of failure of this family of switches be investigated and their structure be studied in order to improve their tolerance level up to 100,000g acceleration ranges. It was found that several factors influence the design and dimensioning of the G-switch or accelerometers, including the following:

- The manufacturing methods of this equipment, as well as the maximum depth of the whole system, limit the amount of minimum dimensions (width, thickness, etc.).
- Both static and dynamic stresses must be below the failure threshold of the material used in construction.
- In addition, a minimum contact force must be created in order to measure the contact between the sensor beams. This force must prevent contact separation.

#### Conflict of Interest Statement

The authors declare no conflict of interest.

#### References

- [1] S. V Kamat, Experimental techniques for the measurement of mechanical properties of materials used in microelectromechanical systems, Def. Sci. J. 59 (2009) 605.

- [2] Q. Zou, W. Tan, E.S. Kim, G.E. Loeb, Single-and triaxis piezoelectric-bimorph accelerometers, *J. Microelectromechanical Syst.* 17 (2008) 45–57.
- [3] C.-L. Dai, P.-H. Kao, Y.-W. Tai, C.-C. Wu, Micro FET pressure sensor manufactured using CMOS-MEMS technique, *Microelectronics J.* 39 (2008) 744–749.
- [4] M. Hautefeuille, C. O'Mahony, B. O'Flynn, K. Khalfi, F. Peters, A MEMS-based wireless multisensor module for environmental monitoring, *Microelectron. Reliab.* 48 (2008) 906–910.
- [5] P.J. Gilgunn, J. Liu, N. Sarkar, G.K. Fedder, CMOS–MEMS lateral electrothermal actuators, *J. Microelectromechanical Syst.* 17 (2008) 103–114.
- [6] S. Gorthi, A. Mohanty, A. Chatterjee, Cantilever beam electrostatic MEMS actuators beyond pull-in, *J. Micromechanics Microengineering.* 16 (2006) 1800.
- [7] G.K. Fedder, R.T. Howe, T.-J.K. Liu, E.P. Quevy, Technologies for cofabricating MEMS and electronics, *Proc. IEEE.* 96 (2008) 306–322.
- [8] B. Shay, T. Hubbard, M. Kujath, Linear frictional micro-conveyors, *Sensors Actuators A Phys.* 148 (2008) 290–298.
- [9] A. Nisar, N. Afzulpurkar, B. Mahaisavariya, A. Tuantranont, MEMS-based micropumps in drug delivery and biomedical applications, *Sensors Actuators B Chem.* 130 (2008) 917–942.
- [10] J. Wang, K.D. Wise, A hybrid electrode array with built-in position sensors for an implantable MEMS-based cochlear prosthesis, *J. Microelectromechanical Syst.* 17 (2008) 1187–1194.
- [11] S. Henry, D. V McAllister, M.G. Allen, M.R. Prausnitz, Microfabricated microneedles: A novel approach to transdermal drug delivery, *J. Pharm. Sci.* 88 (1999) 948.
- [12] T. Liu, C.S. Lough, H. Sehhat, Y. Ming, P.D. Christofides, E.C. Kinzel, M.C. Leu, In-situ infrared thermographic inspection for local powder layer thickness measurement in laser powder bed fusion, *Addit. Manuf.* 55 (2022) 102873. <https://doi.org/10.1016/j.addma.2022.102873>.
- [13] C.-H. Hung, W.-T. Chen, M.H. Sehhat, M.C. Leu, The effect of laser welding modes on mechanical properties and microstructure of 304L stainless steel parts fabricated by laser-foil-printing additive manufacturing, *Int. J. Adv. Manuf. Technol.* 112 (2021) 867–877.
- [14] A. Mahdianikhotbesara, M.H. Sehhat, M. Hadad, Experimental Study on Micro-Friction Stir Welding of Dissimilar Butt Joints Between Al 1050 and Pure Copper, *Metallogr. Microstruct. Anal.* 2021. (2021) 1–16. <https://doi.org/10.1007/S13632-021-00771-5>.
- [15] M.H. Sehhat, · Ali Mahdianikhotbesara, Powder spreading in laser-powder bed fusion process, 23 (2021) 89. <https://doi.org/10.1007/s10035-021-01162-x>.
- [16] M.H. Sehhat, A. Mahdianikhotbesara, M. Hadad, Formability Investigation for Perforated Steel Sheets, *SAE Int. J. Mater. Manuf.* 15 (2022). <https://doi.org/10.4271/05-15-02-0012>.
- [17] M.H. Sehhat, A.T. Sutton, C.-H. Hung, J.W. Newkirk, M.C. Leu, Investigation of Mechanical Properties of Parts Fabricated with Gas- and Water-Atomized 304L Stainless Steel Powder in the Laser Powder Bed Fusion Process, *JOM* 2021. (2021) 1–8. <https://doi.org/10.1007/S11837-021-05029-7>.
- [18] M.H. Sehhat, B. Behdani, C.-H. Hung, A. Mahdianikhotbesara, Development of an Empirical Model on Melt Pool Variation in Laser Foil Printing Additive Manufacturing Process Using Statistical Analysis, *Metallogr. Microstruct. Anal.* 2021. (2021) 1–8. <https://doi.org/10.1007/S13632-021-00795-X>.
- [19] C.-H. Hung, T. Turk, M.H. Sehhat, M.C. Leu, Development and experimental study of an automated laser-foil-printing additive manufacturing system, *Rapid Prototyp. J. ahead-of-print* (2022). <https://doi.org/10.1108/RPJ-10-2021-0269>.
- [20] M.H. Sehhat, J. Chandler, Z. Yates, A review on ICP powder plasma spheroidization process parameters, *Int. J. Refract. Met. Hard Mater.* 103 (2022) 105764. <https://doi.org/10.1016/J.IJRMHM.2021.105764>.
- [21] M.H. Sehhat, A. Mahdianikhotbesara, F. Yadegari, Impact of temperature and material variation on mechanical properties of parts fabricated with fused deposition modeling (FDM) additive manufacturing, *Int. J. Adv. Manuf. Technol.* (2022). <https://doi.org/10.1007/S00170-022-09043-0>.
- [22] T. Liu, C.S. Lough, H. Sehhat, J. Huang, E.C. Kinzel, M.C. Leu, In-Situ Thermographic Inspection for Laser Powder Bed Fusion, in: 2021 Int. Solid Free. Fabr. Symp., University of Texas at Austin, 2021.
- [23] M.H. Sehhat, A.T. Sutton, C. Hung, B. Brown, R.J.O. Malley, J. Park, M.C. Leu, Plasma spheroidization of gas-atomized 304L stainless steel powder for laser powder bed fusion process, 1 (2022).
- [24] A. Mahdianikhotbesara, M.H. Sehhat, M. Hadad, A Numerical and Experimental Study into Thermal Behavior of Micro Friction Stir Welded Joints of Al 1050 and Copper Sheets, *Adv. Mater. Res.* 1170 (2022) 49–60. <https://doi.org/10.4028/P-01AG12>.
- [25] M.H. Sehhat, A. Mahdianikhotbesara, F. Yadegari, Verification of Stress Transformation in Anisotropic Material Additively Manufactured by Fused Deposition Modeling (FDM), (2021). <https://doi.org/10.21203/RS.3.RS-1107949/V1>.
- [26] T. Turk, C.-H. Hung, M. Hossein Sehhat, M.C. Leu, Methods of Automating the Laser-Foil-Printing Additive Manufacturing Process, in: 2021 Int. Solid Free. Fabr. Symp., University of Texas at Austin, 2021.
- [27] F. Yadegari, M.H. Sehhat, A. Mahdianikhotbesara, A Numerical Study of Automotive Body Panel Draw Dies Defects Using Finite Element Simulation, (2022). <https://doi.org/10.21203/RS.3.RS-1300589/V1>.
- [28] M.H. Sehhat, A. Mahdianikhotbesara, F. Yadegari, Experimental Validation of Conductive Heat Transfer Theory: Thermal Resistivity and System Effects, *Comput. Res. Prog. Appl. Sci. Eng.* 7 (2021) 1–6. <https://doi.org/10.52547/CRPASE.7.4.2415>.
- [29] M. Hemmatnezhad, Experimental Vibration Investigation of Annular Plates, *Comput. Res. Prog. Appl. Sci. Eng.* ©PEARL Publ. CRPASE Vol. 01 (2015) 1–7. <http://crpase.com/archive/CRPASE-2015-VOL-01-ISSUE-01-01.pdf>.
- [30] M. Soltaninejad, M. Soltaninejad, K. Farshad Saberi, M.K. Moshizi, V. Sadeghi, P. Jahanbakhsh, Environmental-friendly mortar produced with treated and untreated coal wastes as cement replacement materials, *Clean Technol. Environ. Policy.* 23 (2021) 2843–2860. <https://doi.org/10.1007/S10098-021-02204-X/FIGURES/18>.
- [31] P. Jahanbakhsh, F. Saberi K, M. Soltaninejad, S.H. Hashemi, Laboratory Investigation of Modified Roller Compacted Concrete Pavement (RCCP) Containing Macro Synthetic Fibers, *Int. J. Pavement Res. Technol.* 2022. (2022) 1–15. <https://doi.org/10.1007/S42947-022-00161-2>.
- [32] W.W. Chen, Exploration of MEMS G-Switches at 100-10,000 G-Levels with Redundancy, *PURDUE UNIV LAFAYETTE IN*, 2014.